Astrophys Space Sci (2018) 363:83
https://doi.org/10.1007/s10509-018-3303-4

ORIGINAL ARTICLE

Study of equatorial plasma bubbles using all sky imager and scintillation technique from Kolhapur station: a case study

A.K. Sharma[1] · O.B. Gurav[1] · H.P. Gaikwad[1] · G.A. Chavan[1] · D.P. Nade[2] · S.S. Nikte[3] · R.N. Ghodpage[4] · P.T. Patil[4]

Received: 11 September 2017 / Accepted: 19 March 2018

Abstract The nightglow observations of OI 630.0 nm emission carried out from low latitude station Kolhapur using All Sky Imager (ASI) with 140° field of view (FOV) for the month of April 2011 are used. The images were processed to study the field aligned irregularities often called as equatorial plasma bubbles (EPBs). The present study focuses on the occurrence of scintillation during the traversal of EPBs over ionospheric pierce point (IPP). Here we dealt with the depletion level (depth) of the EPB structures and its effect on VHF signals. We compared VHF scintillation data with airglow intensities at Ionospheric pierce point (IPP) from the same location and found that the largely depleted EPBs make stronger scintillation. From previous literature, it is believed that the small scale structures are present near the steeper walls of EPBs which often degrades the communication, the analysis presented in this paper confirms this belief.

Keywords Equatorial Plasma Bubbles (EPBs) · Depletion level of EPBs · VHF scintillation

✉ O.B. Gurav
omgurav91@gmail.com

A.K. Sharma
aks_phy@unishivaji.ac.in

H.P. Gaikwad
herambgaikwad01@gmail.com

G.A. Chavan
gangadharchavan2@gmail.com

D.P. Nade
dada.nade@gmail.com

S.S. Nikte
nikte.suraj@gmail.com

R.N. Ghodpage
rupeshghodpage@gmail.com

P.T. Patil
ptpiigkop@yahoo.com

1 Space and Earth Science Laboratory, Department of Physics, Shivaji University, Kolhapur, India

2 Department of Basic Sciences & Humanities, Sanjay Ghodawat University, Atigre, India

3 Department of Basic Sciences and Humanities, Fabtech Technical Campus College of Engineering and Research, Sangola, India

4 Medium Frequency Radar, Indian Institute of Geomagnetism, Shivaji University Campus, Kolhapur, India

1 Introduction

Field aligned irregularities (FAIs) are often called as equatorial plasma bubbles (EPBs) have been studied using ground based instruments like All Sky Imager (ASI) from many decades over low latitude stations (Pimenta et al. 2003; Mukherjee 2006; Taori et al. 2010; Rajesh et al. 2010; Ghodpage et al. 2014; Sharma et al. 2014b; Nade et al. 2015). The effect of ionospheric irregularities on radio signals have also been studied by various researchers using GPS (Rama Rao et al. 2006; Haase et al. 2011) and VHF scintillation techniques (Basu et al. 1980; Vijayakumar and Pasricha 1997; Chakraborty et al. 1999; Tiwari et al. 2013). At the post sunset, the lower ionosphere quickly decays, forming a steep density gradient at the base of raised F-region which develops the conditions for a gravitational Rayleigh-Taylor instability. This plasma instability in the lower F region is responsible for the development of EPBs which can grow as they rapidly ascend and align themselves along the magnetic field lines and generate density irregularities in their wake (Wiens et al. 2006). The result is a large region of ionization depletion seen from below (earth) as one or more darkened flux tubes imaged with the OI 630.0 nm

Published online: 29 March 2018

nightglow background emissions called as EPBs. However the three dimensional structure of EPBs are not well understood despite considerable progress. The EPBs seen in the All Sky Images are only the trace of the plasma depletion near the F-peak height (e.g. Kil et al. 2009). Further, the EPB is thought to be a "shell" like structure (Kil 2015) which needs to be modeled using advanced simulation techniques. The equatorial F-region plasma within an entire flux tube becomes unstable and hence the portion of irregularity extends in length up to thousands of km to either side of the magnetic equator (Anderson and Haerendel 1979). Sinha and Raizada (2000) have determined east-west and north-south extension of EPBs using all sky optical imaging technique over SHAR (14°N, 80°E, 5.5°N dip latitude) and conclude that east-west extent of EPBs varied with depletion depth.

Understanding the internal dynamics and morphology of EPBs is important because they affect the radio waves causing scintillation which degrades the performance in communication and navigation systems. The depleted density in the ionosphere inside the volume of the bubble very often produces rapid changes both in amplitude and phase of the signal passing through the bubble; this phenomenon is called ionospheric scintillation (Dandekar and Groves 2004). The occurrence of scintillation at any station situated off the magnetic equator depends on the height to which EPBs develops under E × B (Kumar and Gwal 2000). The geometry of apex height and ray path for the present location (Kolhapur; 16.8°N, 74.2°E, 10.6° dip lat.) indicates that the EPBs must grow over magnetic equator to about 300 to 400 km to produce scintillation at this station. Vijayakumar and Pasricha (1997) reported the plasma bubble induced (PBI) scintillations using signals from the geostationary satellite FLEETSAT (73°E) at Delhi (28.6°N, 77.2°E) during March-April 1991.

In present study we have used All Sky Imager (ASI) with OI 630.0 nm emission to observe EPBs and VHF scintillation data of 251 MHz to study the effect of EPBs on the strength of scintillation. We have compared the airglow intensity recorded in the ASI images at 630.0 nm emission with that of scintillation index at IPP. For this work we have determined the position of ionospheric pierce point (IPP) which is the point in the ASI image (or in airglow emission layer at 250 km altitude) through which satellite signals are penetrating and reaching the receiver at Kolhapur (refer Fig. 1). The airglow intensities at IPP varies with scintillation index, the results of which are discussed in the present paper.

2 Instrumentation

2.1 All Sky Imager (ASI)

A high resolution ASI consists of different interference filters having central wavelengths of OI 630.0 nm, OI

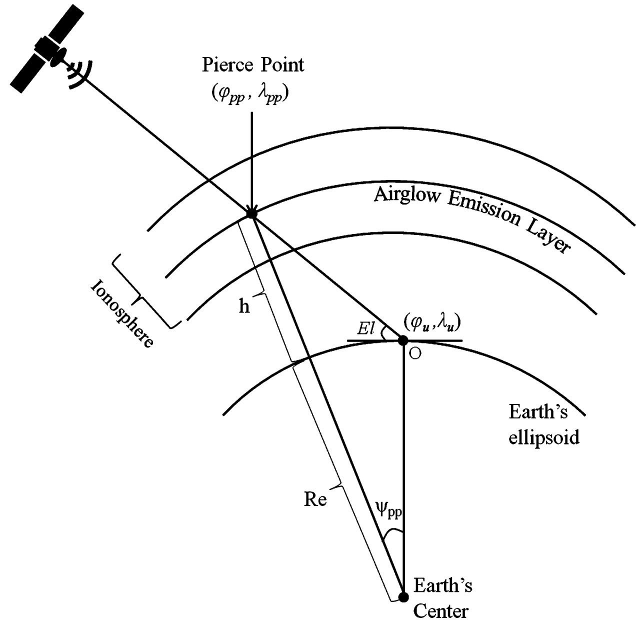

Fig. 1 The geometry for the determination of Ionospheric Pierce Point (IPP)

557.7 nm and OH Meinel bands (720.0 nm–910.0 nm). The fish eye lens (f/4 Mamiya RB67) having focal length of 24 mm, collects the light from the night sky over a field of view (FOV) of 140°. It covers a zenith angle range of about 70° which corresponds to horizontal distance of about nearly 1220 km diameter at an altitude of 250 km. The CCD detector having quantum efficiency greater than 95% with an array of 1024 × 1024 pixels with 16 bits resolution is used in ASI. The CCD is thermoelectrically cooled (−80 °C) to reduce dark signals before the operation. The observations have been taken for 7 nights before and after the new moon night. The detailed specification of ASI installed at Kolhapur station has been briefly introduced by Sharma et al. (2012), Nade et al. (2013) and Patil et al. (2016). The images of ASI give the morphology of EPBs which are useful in the study of ionosphere.

2.2 VHF scintillation

The regular observations of amplitude scintillation with 251 MHz radio signal transmitted by UFO2 geostationary satellite (positioned at 71.2°E) has been carried out since last few years at Kolhapur. Two identical receivers with eleven element Yagi-Uda antennae spaced 300 m apart in magnetic east-west direction is installed at Kolhapur. The ionospheric scintillations are digitally recorded at sampling rate of 20 Hz. Scintillations in the radio signal are obtained by a parameter called S_4-index (S_4), the root mean squared standard deviation of intensity of the signal which indicates the strength of amplitude scintillation (Wernik et al. 2004). The measured average intensities at IPP are compared with the scintillation index (S_4) obtained from VHF scintillation data. When radio signals passes through the medium in the ionosphere, a rapid change in its phase and amplitude is observed. The quantity used to calculate the strength of such random fluctuations in the radio signals is termed as scintillation index. It is given by the equation,

$$S_4^2 = \frac{\langle I^2 \rangle - \langle I \rangle^2}{\langle I \rangle^2}$$

Where, I represent the intensity of the signal.

2.3 Ionosonde

The ionosonde at Tirunelveli (8.7°N, 77.8°E) is a vertical incidence Canadian Advanced Digital Ionosonde (CADI). It sweeps the radio frequency from 1 MHz to 30 MHz with a height resolution of 6 km (Taori et al. 2015). In the present analysis, we study the VHF scintillation occurred at low latitude. Ionosonde data are used here to check whether VHF scintillation occurred under spread condition or not.

3 Geometry to calculate Ionospheric Pierce Point (IPP)

The signal transmitted from the satellite to the receiver penetrates the ionospheric shell (F-layer peak), the intersection between line of sight and this shell is called the ionospheric pierce point (IPP). Rama Rao et al. (2006) studied the F-layer peak height variation using GPS data over Indian low latitude region and found that the peak electron density height (hpF2) varies from about 275 to 575 km at the equatorial region, and varies slightly from 300 to 350 km at and beyond the anomaly crest regions. Here we have assumed that the OI 630.0 nm emission peak height for Kolhapur location is around 250 km (Ghodpage et al. 2014). In present analysis we have calculated the geodetic coordinates of IPP at this altitude. Figure 1 represents the geometry for determination of IPP coordinates. The VHF scintillation receiver is located at point 'O' having coordinates (φ_u, λ_u) which represents the latitude and longitude of the location (16.8°N, 74.2°E, 10.6° dip. Lat.), El is the elevation angle to the satellite, R_e is the radius of the earth (∼6371 km), h is the height of airglow emission layer (∼250 km), ψ_{pp} is the earth's centered angle between the receiver and IPP and (φ_{pp}, λ_{pp}) are the coordinates of the IPP.

The mathematical equations to calculate the coordinates of IPP are described by Park et al. (2004) as follows,

$$\psi_{pp} = \frac{\pi}{2} - El - \sin^{-1}\left(\frac{R_e}{R_e + h}\cos El\right) \quad (1)$$

$$\varphi_{pp} = \sin^{-1}(\sin\varphi_u \cos\psi_{pp} + \cos\varphi_u \sin\psi_{pp}\cos A) \quad (2)$$

$$\lambda_{pp} = \lambda_u + \sin^{-1}\left(\frac{\sin\psi_{pp}\sin Az}{\cos\varphi_{pp}}\right) \quad (3)$$

Now, the elevation angle (El) and azimuth angle (Az) of the satellite can be computed using the following equations,

$$Az = 180° + \tan^{-1}\left[\frac{\tan G}{\tan L}\right] \quad (4)$$

Where, G = difference between satellite orbital position (i.e. satellite longitude) and the receiver longitude and L = latitude of the receiver.

Also if the satellite orbital location is in east (E), then,

G = Receiver longitude

− Satellite orbital position (i.e. satellite longitude).

In present case, the satellite UFO2 is a geostationary satellite positioned at 71.2°E which is the longitude of the satellite.

So, $G = 74.2°\text{E} - 71.2°\text{E} = 3°$

Therefore,

$$Az = 180° + \tan^{-1}\left[\frac{\tan 3°}{\tan 16.8°}\right] = 189.8° \quad (5)$$

Now,

$$El = \tan^{-1}\left[\frac{\cos G\cos L - 0.1512}{\sqrt{1 - \cos^2 G\cos^2 L}}\right]$$

(Here, 0.1512 is a constant) (6)

$$El = \tan^{-1}\left[\frac{\cos 3°\cos 16.8° - 0.1512}{\sqrt{1 - \cos^2 3°\cos^2 16.8°}}\right] = 69.97° \quad (7)$$

By putting the values of azimuth angle and elevation angle in Eq. (1) we get,

$\psi_{pp} = 0.79°$

Finally, putting the values of Az, El and ψ_{pp} in Eqs. (2) and (3), the coordinates of IPP (φ_{pp}, λ_{pp}) can be calculated which comes out to be,

$\varphi_{pp} = 16.02°$ and $\lambda_{pp} = 74.06°$.

Please refer Fig. 2(a) for the representation of coordinates of IPP on latitude-longitude grid of all-sky image at 250 km altitude.

4 Method of data analysis

4.1 Comparison of airglow intensities and S_4 index at IPP

The data of OI 630.0 nm emission recorded by ASI for the month of April 2011 are used for the present study. Out

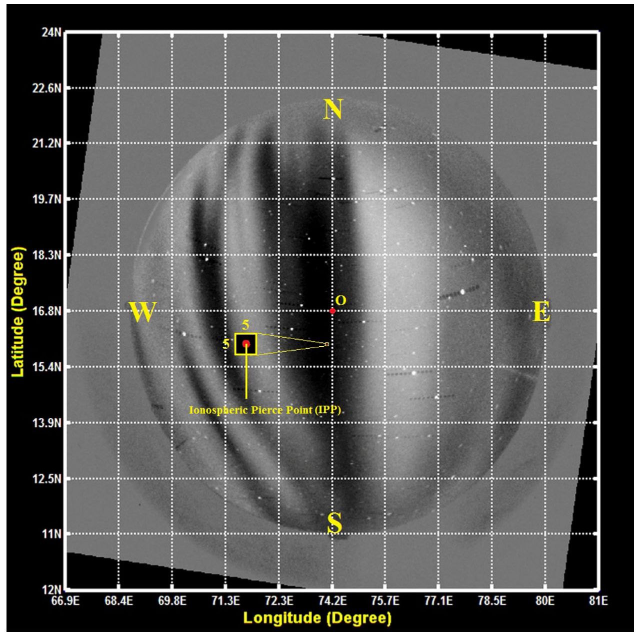

(a)

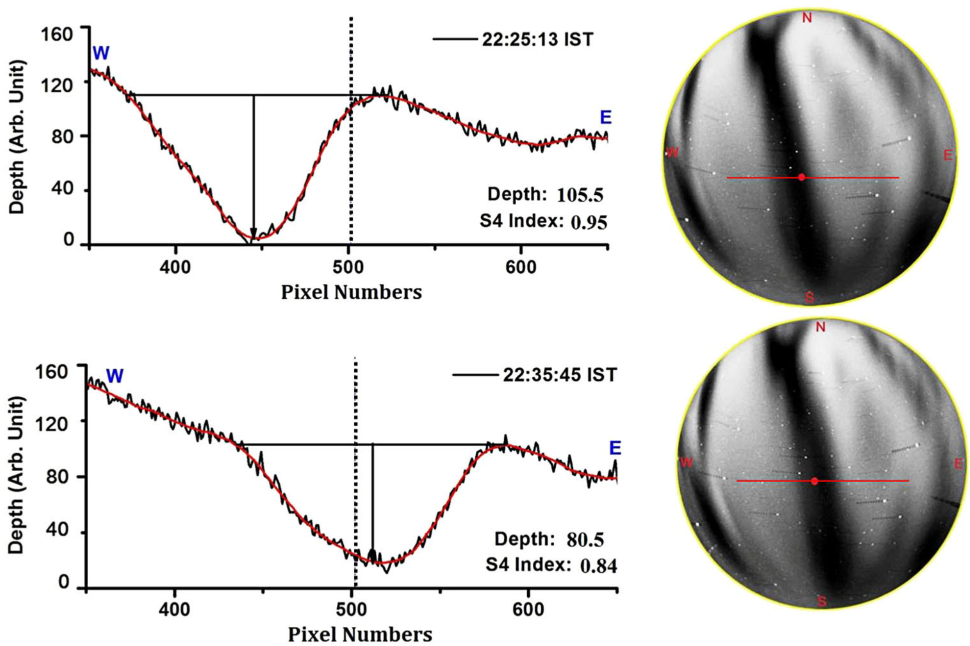

(b)

Fig. 2 (**a**): Mapping of IPP coordinates onto the OI 630 nm airglow image recorded from Kolhapur. The geographic latitudes and longitudes covered in the image are given respectively in left and bottom axis. The point 'O' is the zenith which is the location of all sky imager and VHF scintillation receiver. The position of IPP (16.02°N, 74.06°E) is shown in the Figure. The magnified rectangle of 5 × 5 pixels contains the red filled circle which is the location of IPP in the ASI image.
(**b**): Measurement of depth using scanning method for the EPBs which occurred over IPP (vertical dotted line in left panel)

of 13 nights observations only 9 nights shows signature of EPBs and 6 nights having significant occurrence are used for the present study. The raw data of ASI have been processed by using various image processing methods reported by Garcia et al. (1997), Pimenta et al. (2001), Sharma et al. (2014a) and Sivakandan and Taori (2015). However we have used averaging method described by Sharma et al. (2014a) to process all sky images. Each all sky image is composed of 1024 × 1024 (∼1MP resolution) pixels. The latitude-longitude shown in Fig. 2(a) are converted into kilometer by considering 1 pixel = 1.533 km (Sharma et al. 2014a). After locating the coordinates of IPP, we have measured the average intensity of 5 × 5 square bin of OI 630.0 nm images at IPP as shown in Fig. 2(a).

4.2 Determination of depletion level (depth) of EPBs over IPP

As a case study we have considered six night's data from April month because images of OI 630.0 nm showing very

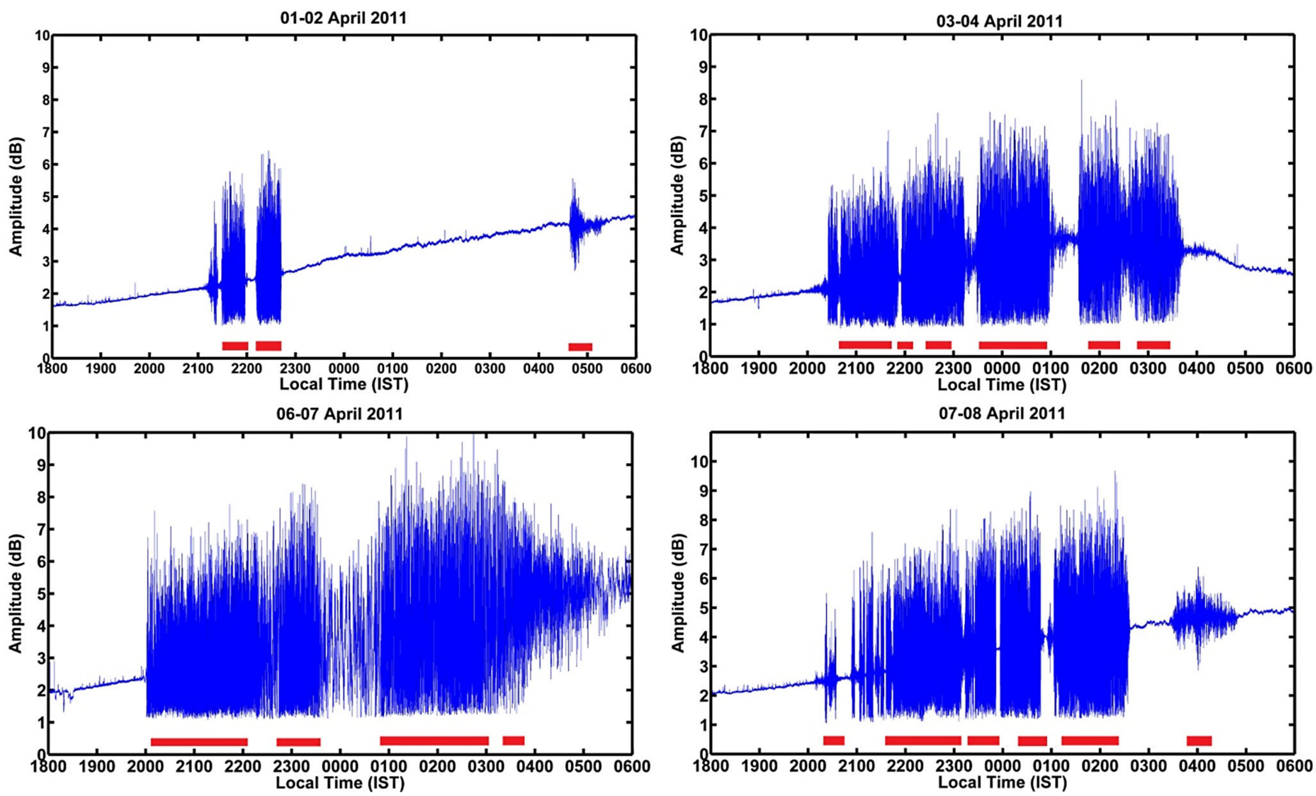

(a)

Fig. 3 (**a**): Amplitude scintillation data for the night of 01–02, 03–04, 06–07 and 07–08 April 2011. The red rectangle at the bottom of each panel indicates the occurrence of EPBs in OI 630.0 nm images. (**b**): Simultaneous measurement of absolute average intensity gradient of 5 × 5 square bin in OI 630.0 nm emission and scintillation index (S4) at IPP for the nights of 01–02, 03–04, 06–07 and 07–08 April 2011

good data quality, fully developed structures of EPBs, during these nights which are suitable to study the depletion level. Here we calculate depth of depletion of EPBs by taking ratio of depleted region to the background (Sinha and Raizada 2000). We retrieve intensity data with pixel values from each image of OI 630.0 nm by scanning it through IPP in east west direction. Figure 2(b) illustrates intensity variations with pixel values in left panel while in right panel shows the scanning of corresponding images. In right panel red line and dot is showing the east-west scan and position of IPP on image of OI 630.0 nm respectively. The vertical dotted line in the left panel corresponds to the red dot in the images in right panel. In left panel, the lowest intensity region indicates the depleted area over low latitude F region. Thus herein we have calculated the depth of EPB by taking difference between background intensity and lowest intensity in arbitrary unit. The downward arrow in the left panel gives the depletion depth (in terms of Arb. Unit).

5 Results and discussion

The aim of the present paper is to study the occurrence of scintillation and its variation during the traversal of EPBs. For this, initially we compared the raw amplitude scintillation data for the corresponding nights with the occurrence of EPBs over IPP as shown in Fig. 3(a). In Fig. 3(a) the blue curve (or patches) indicates the amplitude scintillation recorded at Kolhapur location and the red rectangles at the bottoms of each panel indicates the occurrence of EPBs during that period. It can be seen that, when EPBs crosses the IPP, suddenly scintillation encounters which is seen as the patches in amplitude data. This suggest that the presence of EPBs over IPP causes scintillation. Apart from the raw data, we further calculated scintillation index as described in Sect. 2.2 and compared it with the corresponding airglow intensity at IPP. The images of ASI are cropped with 5 × 5 square bin around IPP for the whole night and the average intensities of these square bins are measured. Further we take absolute gradient of these intensities and compared with the corresponding S_4 index obtained from VHF scintillation data for the nights of 01–02, 03–04, 06–07 and 07–08 April 2011 as shown in Fig. 3(b). The red downward arrows are marked from the downward peaks (S_4 minima's) of the S_4 index curve (blue line) which coincides with the lower values of absolute intensity gradient. The downward peaks in the absolute intensity gradient curves are the signatures of EPBs. The red downward arrows drawn from the S_4

Fig. 3 (*Continued*)

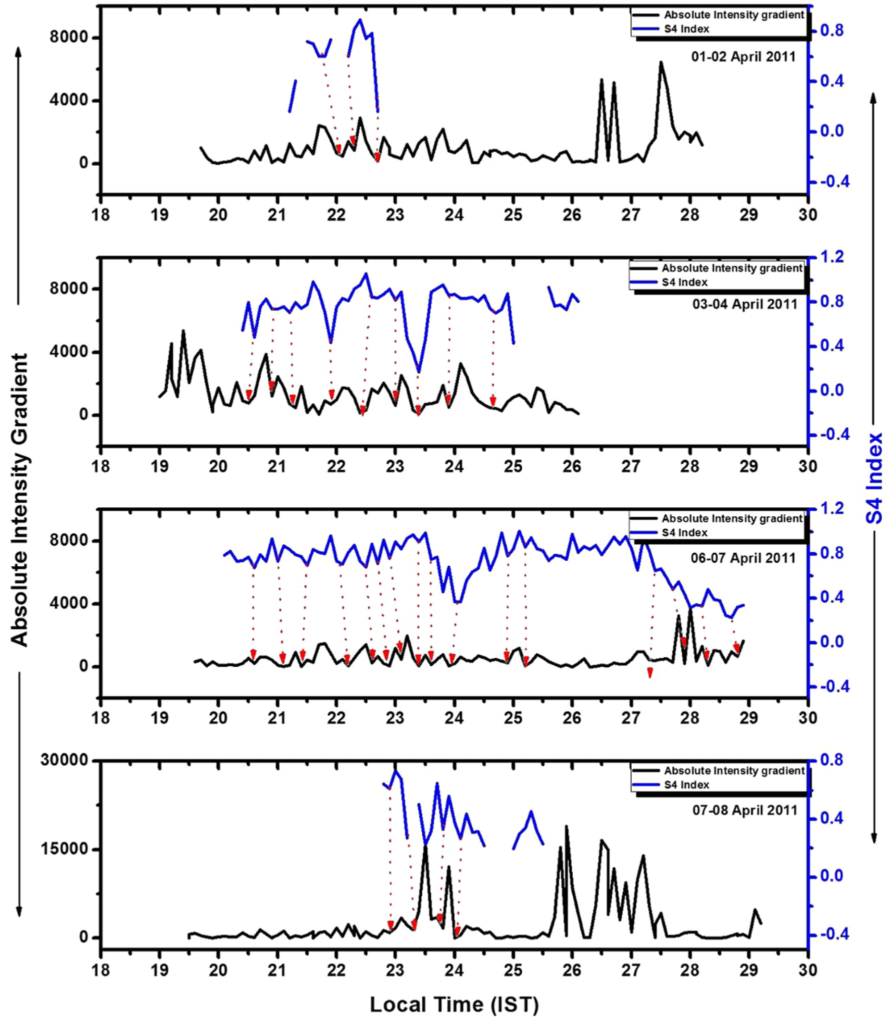

(b)

minima's intersect with the absolute intensity gradient curve at the center of EPBs. This means that the scintillation is minimum at the center and it increases towards the edges of EPBs. Here, the red arrows drawn are not exactly perpendicular to the absolute intensity gradient curve, they are somewhat tilted. So, there occurs a lag in the S_4 minima's and the center of EPBs. This is because, the OI 630.0 nm emission peak height for Kolhapur location is assumed to be around 250 km (Ghodpage et al. 2014). In this context, the EPBs can only be visible when it comes to an altitude of 250 km. So that it makes a footprints in all sky images. Only bottom structure of EPBs are observed in OI 630.0 nm emission images. Because optical observation can detect the EPBs only near the F-peak height where the airglow emission rate is maximum in the night time. The EPBs seen in the All Sky Images are only the trace of the plasma depletion shell near the F-peak height (e.g. Kil et al. 2009). If EPB is on the top of the peak then it will not appear in all sky images captured in OI 630.0 nm emission. However, the signatures of EPBs can be confirmed by other radio techniques such as GPS, VHF scintillation etc. In VHF scintillation technique the average distance of irregularity (small scale) from ground is considered to be around 350 km (Tulasi Ram et al. 2009). So the lag between the intensity and S4 index in Fig. 3(b) is might be due to difference in the altitude.

To understand this phenomenon in detail we studied the condition of the ionosphere during the nights of 04–05 April 2011 and 05–06 April 2011. Figures 4 and 5 represents the simultaneous measurements of absolute intensity gradient in OI 630.0 nm emission at IPP in ASI image (bottom panel), scintillation index (S_4) (middle panel), virtual height (h'f) and $(f_o\text{F2})^2$ (upper two panels) for the night of 04–05 April 2011 and 05–06 April 2011 respectively. For the intensity we have cropped ASI images at IPP in 5 × 5 pixels rectangle and averaged its intensity. Further the absolute gradient in these intensities for the corresponding nights has been estimated. The deep minima's in the absolute intensity gradient (B1, B2 etc.) plotted in the bottom panel of

Fig. 4 Simultaneous measurement of absolute average intensity gradient of 5 × 5 square bin in OI 630.0 nm emission, scintillation index (S_4) at IPP point, virtual height (h'f) and f_oF2 derived from ionosonde data for the night of 04–05 April 2011

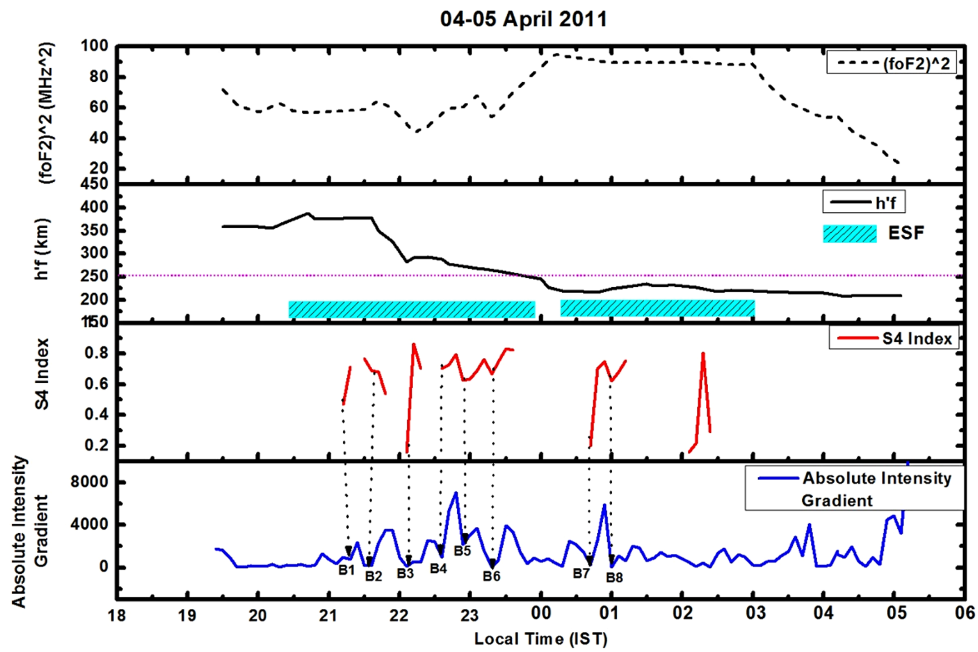

Fig. 5 Same as Fig. 4 but for the night of 05–06 April 2011

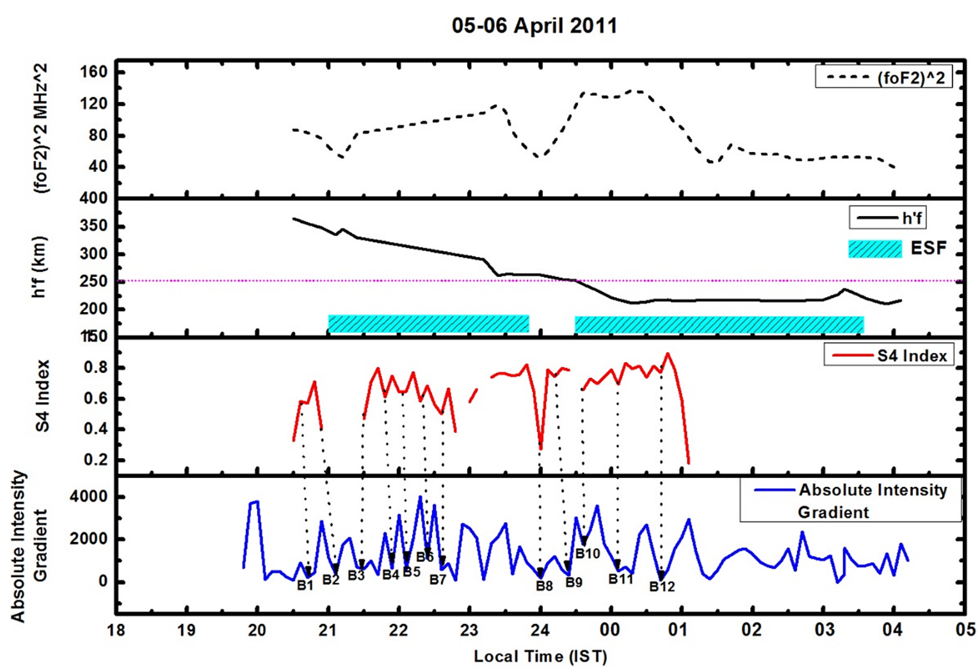

Figs. 4 and 5 indicate the center of EPBs. The scintillation index (red curve) is calculated from VHF scintillation data and plotted against the local time. The scintillation index (S_4) equal to or greater than 0.6 indicates the strong bubble activity (Dandekar and Groves 2004). The spread-F activities are depicted by horizontal cyan colored bands. It is well known that the square of the parameter f_oF2 is proportional to the electron density (N_{max}) at the peak of the F2 layer (Mukherjee 2006). The $(f_o\text{F2})^2$ and h'f curves are smoothed by 5 point average to get the continuity. The horizontal pink dotted line in h'f curve is the airglow emission peak height (∼250 km). In Fig. 4, the dotted lines are drawn from the S_4 minima's which rests at the EPBs center (B1 to B8) in the intensity curve. This shows that the S_4 is minimum inside the EPBs and it increases towards the edges. That means the increase in S_4 index is indeed occurred due to traversal of EPBs. Also, there is a notable lag in the matching of the minima's in both the curves. This is due to altitude difference in both the techniques as described in Sect. 5, first paragraph. In Fig. 4, h'f attains its maxima around 21:00 IST and decreased towards dawn period. Also it remained quite steady (in between 200 to 250 km) up to dawn period. Also

$(f_o\text{F2})^2$ is increased from 23:00 IST and decreased towards dawn periods.

Yeh et al. (1979) observed scintillation patches associated with the depletions in total electron content (due to EPBs) over Natal, Brazil (35.23°W, 5.85°S, dip −9.6°). They concluded that the amplitude scintillations were occurred during the traversal of VHF signals through EPBs. In Fig. 5, the center of S_4 minima's coincides with the centers of EPBs (B1 to B12). Further, between 21:40 IST to 23:00 IST four EPBs (Multiple depletions) were observed as B4, B5, B6 and B7 which matches to the corresponding S_4 minima's as shown by dotted arrows. This states that the scintillation occurs indeed due to presence of EPBs in the line of site of the incoming signal. The virtual height (h'f) remained quite steady after midnight. The density outside the EPBs in all sky images were quite increased (not shown in Figures) when the h'f is found to be around ∼250 km (±50) where airglow emission rate is maximum. This makes the density gradient towards the edges of EPBs which are harmful for VHF signal performance rather than at the center of EPBs. For the generation of small scale irregularities the ambient density (n_o) of the ionosphere is also important along with the density variation (n_e) inside the EPB structure (Banola et al. 2005). Also it is believed that the small scale structures are absent in non-ESF nights (Seker and Chakrabarty 2008), however the scintillation peaks obtained in Figs. 4 and 5 are under ESF events. Haase et al. (2011) showed that GPS TEC and corresponding S_4 index are correlated with each other. Also he found some noteworthy relationship between airglow intensity derived from ASI images and S_4 index derived from GPS.

As mentioned in Sect. 4.2, we have measured the depth of each EPBs which appeared over IPP and compared this with corresponding scintillation index for the nights of 04–05 April 2011 and 05–06 April 2011. These nights were magnetically quite ($\sum Kp < 30$). The measurements are depicted in Table 1. From the previous literature, it is believed that the small scale structures are present near the steep walls of EPBs which often degrades the communication (Dandekar and Groves 2004). It can be seen from Table 1 that, largely depleted EPBs produces stronger scintillation (>0.6). Here we suggest that, the small scale structures might be abundantly available inside the largely depleted EPBs which becomes the cause for the stronger scintillation. Banola et al. (2005) reported that the S_4 indices and fade rates are higher during evolution phase of EPBs. The EPBs which are at fully developed stage, consists large depletion level which can cause strong scintillation.

The present analysis can be used to study the scintillation activity inside the EPBs which are traversed over IPP. For this, we have considered a single EPB journey for the night of 04–05 April 2011 and 05–06 April 2011 which appeared over IPP and compared this with its corresponding S_4 indices as shown in Fig. 6(a) and (b). These are the

Table 1 The measured depths of EPB structures appeared over IPP and their corresponding S_4 indices for the nights of 04–05 April 2011 and 05–06 April 2011

04–05 April 2011			05–06 April 2011		
Time (IST)	S_4 Index	Depth (Arb. Unit)	Time (IST)	S_4 Index	Depth (Arb. Unit)
21:53	0.4392	62.33	21:48	0.6134	52.16
21:58	0.8111	80.34	21:54	0.75	67.82
22:04	0.8238	88.55	22:17	0.7256	77.92
22:09	0.8352	89.66	22:23	0.6878	44.37
22:14	0.7943	79.59	22:28	0.5683	48
22:25	0.9553	144	22:34	0.6608	52.71
22:30	1.0556	121.25	22:40	0.8104	98.65
22:35	0.8458	118.75	22:46	0.6793	68.55
22:41	0.8381	98.75	22:57	0.5789	55.67
23:38	0.8471	126.25	23:32	0.8497	104.5
23:44	0.7558	113.75	23:38	0.7912	79.17
23:49	0.9572	103.33	0:58	0.7815	44.17
23:54	0.8596	90.62	1:33	0.7246	33.75
0:00	0.8696	109.58	1:39	0.7586	42.09
0:05	0.837	77.91	1:44	0.7707	44.37

east-west scans through IPP and the intensities are plotted against pixel numbers for different local time. The intensity of OI 630.0 nm emission is retrieved by scanning of image through IPP in east-west direction, this intensity data is smoothed by 50 points averaged for further analysis. In Fig. 6(a), initially at 23:38:54 IST the EPB enters from west over IPP (shown by blue vertical dotted line) where S_4 index is 0.83 at east wall. In the next moment, at 23:44:10 IST, the S_4 becomes maximum as 0.85. As time goes the EPB moves eastward, at instant when radio signals are exactly penetrated the EPB through its center (at 23:49:26 IST), the S_4 is lesser (0.79) comparatively. Finally, when the signals interfere with western wall of EPBs at 00:05:14 IST, the S_4 index attains maximum value (0.97). Also in Fig. 6(b), the same case observed that the S_4 index was minimum when EPBs center (at 01:50:25 IST) lies exactly at the IPP and it was maximum towards the edges. The edges of EPBs has larger density gradient than at the center. As we go towards the edges from the center then density (intensity in images) varies remarkably. The present analysis uses the point in the all sky image where VHF signals are penetrating and the scintillation activity inside, near edges and outside the EPBs can be studied. From Fig. 6(a) and (b) it is confirmed that the scintillation is higher at or near the steeper walls of EPBs than at the center.

Further, we have checked the variation in drift velocities of the small scale irregularities (obtained from VHF scintillation data) and large scale irregularities (EPBs) imaged in ASI using OI 630.0 nm emission. By comparing the posi-

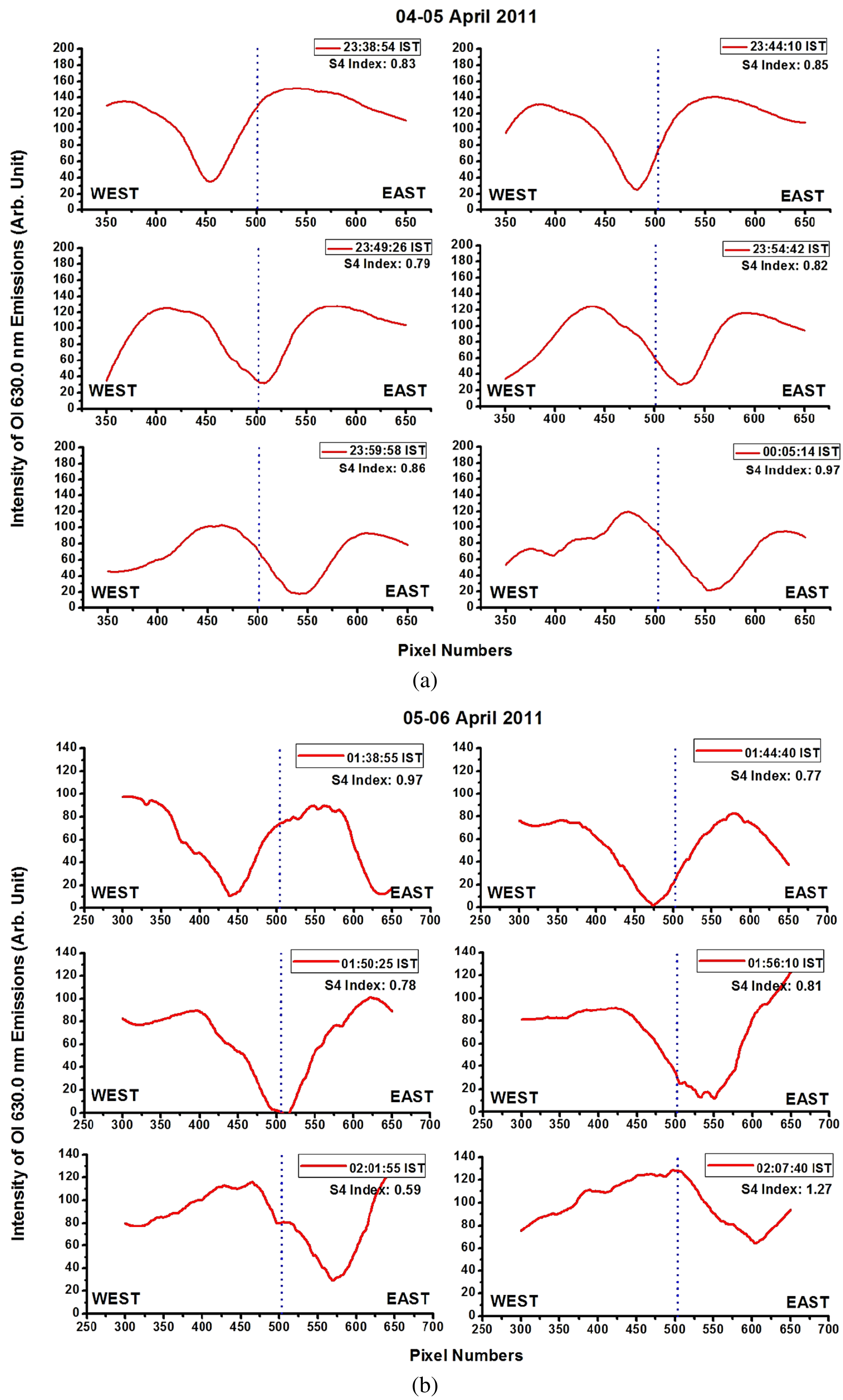

Fig. 6 (**a**): Depth of a single EPB occurring over IPP for the night of 04–05 April 2011. The vertical blue dotted line indicates the position of IPP. (**b**): Same as Fig. 6(a) but for the night of 05–06 April 2011

tions of EPBs in consecutive ASI images, the longitudinal offset in terms of pixels can be determined. Further the pixels can be converted into a kilometer which gives the distance travelled by the EPBs. The time difference between consecutive images is around 00:06 minutes. Hence the velocity can be easily determined. The velocity is plotted by

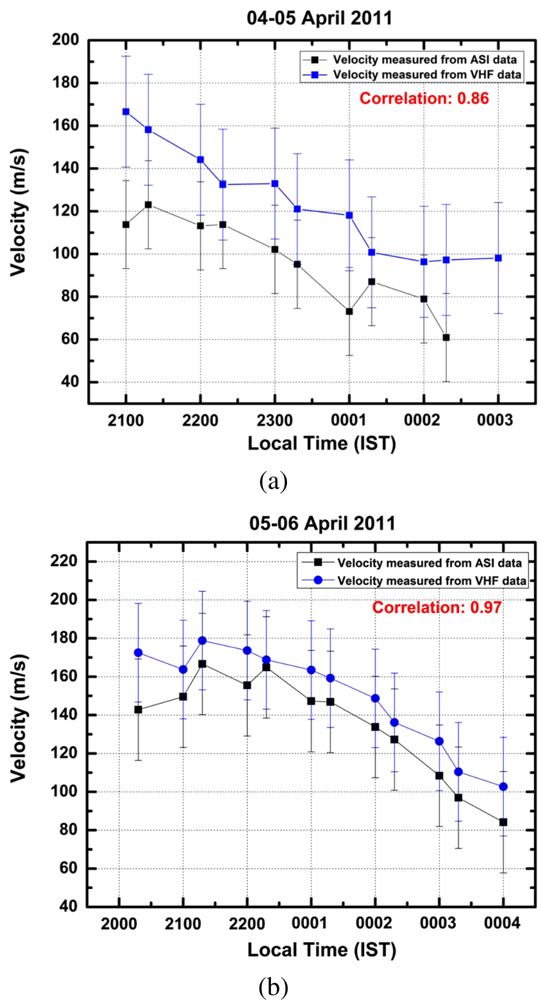

Fig. 7 (**a**): Zonal drift velocity of EPBs calculated from OI 630.0 nm images and VHF scintillation data for the night of 04–05 April 2011. (**b**): Same as Fig. 7(a) but for the night of 05–06 April 2011

taking average of half hour data points throughout the night. The velocity calculated from ASI technique is shown in Fig. 7(a) and (b) for the nights of 04–05 April 2011 and 05–06 April 2011 respectively. The vertical bars depict the standard deviation error. Also, the drift of smaller scale irregularities is determined by VHF scintillation data recorded at Kolhapur. This drift velocity is determined by cross correlation technique introduced by Briggs (1984) and developed by Bhattacharyya et al. (2001). By using this method velocity of each three minutes interval has been determined first and then averaged for 30 minutes. The velocity calculated from VHF scintillation technique is shown in Fig. 7(a) and (b) for the nights of 04–05 April 2011 and 05–06 April 2011 respectively. Bhattacharyya et al. (2001) reported the estimated average value of drift to be 151.9 m/s using amplitude scintillation at 244 MHz from Ancon (11.8°S, 77.2°W, dip latitude 0.9°N). Ghodpage et al. (2014) reported that the average plasma drift velocity calculated from ASI varies between 123–181 m/s for Kolhapur. Also, Patil et al. (2016) determined the velocity using ASI for the same location and observed that the EPB drift velocity varies between 70–200 m/s just ∼2 h after sunset and it gradually decreases towards dawn periods. We found the average drift velocity obtained from ASI and VHF data to be 96.1 ± 20 and 124.1 ± 25 respectively for the night of 04–05 April 2011 and it is found to be 139.9 ± 26 and 154.7 ± 25 respectively for the night of 05–06 April 2011. These calculated zonal velocities are in good agreement with the previously reported literature. Also, we observe that the velocities determined by both the techniques are same in direction but somewhat different in magnitude. The difference in their magnitude might be occurred due to vertical shear in the zonal plasma drift. The effect of this shear in zonal plasma drift in the context of F-region irregularities is investigated by Satyanarayana et al. (1984). Also, the drifts of smaller scale irregularities (determined by VHF technique) were high on both the nights than that of the larger scale irregularities (EPBs).

6 Concluding remarks

The outcomes of the present study are listed below.

1. The specialty of the present paper is that, by observing the depletion level and the position of EPBs at IPP, one can determine how severely the radio signals (e.g. VHF) are degrading at a particular region.
2. In our observation days, the scintillation occurs indeed due to the traversal of EPBs over IPP. This has been confirmed from the minima's of S_4 index matches with the minima's of EPBs intensities (Figs. 4 and 5) and also it is confirmed from Fig. 3(b).
3. The depth and S_4 index correlates with each other. We observed that, largely depleted EPBs produce stronger scintillations (Table 1). On the basis of this observation, we suggest that there might be stronger presence of smaller scale size structures at or near the edges of EPBs (with larger depth) which produces stronger scintillation.
4. The zonal drift measured from both the techniques are different in magnitude throughout night but same in direction moving eastward. The difference in magnitude is might be due to vertical shear in the zonal plasma drift.
5. From previous literature it is believed that the steeper walls of EPBs often degrade the communication. In our study we also found that the S_4 index is higher near edges than at centers of EPBs. This means that the steeper wall of EPBs causes stronger scintillations. We are planning to study this aspect in detail with larger data sets for quite nights in future.

Acknowledgements The observations of OI 630.0 nm emissions were carried out using ASI over Kolhapur under the scientific collaboration between Shivaji University, Kolhapur (S.U.K.) and Indian Institute of Geomagnetism (I.I.G.), Navi Mumbai, India. One of the authors

Mr. O. B. Gurav is thankful to UGC-BSR for financial support (*F.25-1/2014-15(BSR)/7-167/2009/BSR, October 2015*). We are thankful to Dr. B. Kakad for providing VHF scintillation data over Kolhapur. We are also thankful to Dr. S. Sripathi for providing ionosonde data over Tirunelveli and Mr. Amol Valkunde for fruitful discussion in working out the geometry to calculate Ionospheric pierce point (IPP).

References

Anderson, D., Haerendel, G.: J. Geophys. Res. **84**, 4251 (1979)

Banola, S., Pathan, B.M., Rao, D.R.K., Chandra, H.: Earth Planets Space **57**, 47 (2005)

Basu, S., McClure, J.P., Basu, Su., Hanson, W.B., Aarons, J.: J. Geophys. Res. Space Phys. **85**, 5119 (1980)

Bhattacharyya, A., Basu, S., Groves, K.M., Valladares, C.E., Sheehan, R.: Geophys. Res. Lett. **28**, 119 (2001)

Briggs, B.H.: In: Middle Atmos. Progr. Handb. MAP, vol. 13, p. 166 (1984)

Chakraborty, S.K., Das Gupta, A., Ray, S., Banerjee, S.: Radio Sci. **34**, 241 (1999)

Dandekar, B.S., Groves, K.M.: Radio Sci. **39**, 1 (2004)

Garcia, F.J., Taylor, M.J., Kelley, M.C.: Appl. Opt. **36**, 7374 (1997)

Ghodpage, R.N., Taori, A., Patil, P.T., Gurubaran, S., Sripathi, S., Banola, S., Sharma, A.K.: J. Atmos. Sol.-Terr. Phys. **121**, 196 (2014)

Haase, J.S., Dautermann, T., Taylor, M.J., Chapagain, N., Calais, E., Pautet, D.: Adv. Space Res. **47**, 1758 (2011)

Kil, H.: J. Astron. Space Sci. **32**, 13 (2015)

Kil, H., Heelis, R.A., Paxton, L.J., Oh, S.-J.: J. Geophys. Res. **114**, A11302 (2009)

Kumar, S., Gwal, A.K.: J. Atmos. Terr. Phys. **62**, 157 (2000)

Mukherjee, G.K.: Earth Planets Space **58**, 623 (2006)

Nade, D.P., Sharma, A.K., Nikte, S.S., Patil, P.T., Ghodpage, R.N., Rokade, M.V., Gurubaran, S., Taori, A., Sahai, Y.: Ann. Geophys. **31**, 2077 (2013)

Nade, D.P., Shetti, D.J., Sharma, A.K., Taori, A., Chavan, G.A., Patil, P.T., Ghodpage, R.N., Gurav, O.B., Nikte, S.S.: Adv. Space Res. **56**, 1901 (2015)

Park, J.U., Choi, B.K., Lim, H.C., Park, P.H.: Presented at GNSS 2004 International Symposium on GNSS/GPS Sydney, Australia, 6–8 December (2004)

Patil, P.T., Ghodpage, R.N., Taori, A.K., Patil, R.P., Gurubaran, S., Nikte, S.S., Nade, D.P., Sharma, A.K., Banola, S., Narayanan, V.L., Siingh, D.: Ann. Geophys. **59**, A0214 (2016). https://doi.org/10.4401/ag-6868

Pimenta, A.A., Fagundes, P.R., Bittencourt, J.A., Sahai, Y., Gobbi, D., Medeiros, A.F., Taylor, M.J., Takahashi, H.: Adv. Space Res. **27**, 1219 (2001)

Pimenta, A.A., Fagundes, P.R., Sahai, Y., Bittencourt, J.A., Abalde, J.R.: Ann. Geophys. **21**, 2315 (2003)

Rajesh, P.K., Liu, J.Y., Sinha, H.S.S., Banerjee, S.B.: J. Geophys. Res. Space Phys. **115**, 2 (2010)

Rama Rao, P.V.S., Niranjan, K., Prasad, D.S.V.V.D., Gopi Krishna, S., Uma, G.: Ann. Geophys. **24**, 2159 (2006)

Satyanarayana, P., Guzdar, P.N., Huba, J.D., Ossakow, S.L.: J. Geophys. Res. **89**, 2945 (1984)

Seker, R., Chakrabarty, D.: Indian J. Radio Space Phys. **37**, 7 (2008)

Sharma, A.K., Nade, D.P., Nikte, S.S., Ghodpage, R.N., Patil, P.T., Rokade, M.V., Vhatkar, R.S.: Int. J. Eng. Sci. Res. **3**, 746 (2012)

Sharma, A.K., Nade, D.P., Nikte, S.S., Ghodpage, R.N., Patil, P.T., Rokade, M.V., Vhatkar, R.S., Gurubaran, S.: Curr. Sci. **106**, 1085 (2014a)

Sharma, A.K., Nade, D.P., Nikte, S.S., Patil, P.T., Ghodpage, R.N., Vhatkar, R.S., Rokade, M.V., Gurubaran, S.: Adv. Space Res. **54**, 435 (2014b)

Sinha, H.S.S., Raizada, S.: Earth Planets Space **52**, 549 (2000)

Sivakandan, M., Taori, A.: Earth Sci. India **8**, 50 (2015)

Taori, A., Makela, J.J., Taylor, M.: J. Geophys. Res. Space Phys. **115**, 1 (2010)

Taori, A., Parihar, N., Ghodpage, R., Dashora, N., Sripathi, S., Kherani, E.A., Patil, P.T.: J. Geophys. Res. Space Phys. **120** (2015). https://doi.org/10.1002/2015JA021541

Tiwari, S., Sarkar, S., Vishwakarma, A., Gwal, A.K.: Adv. Phys. Theor. Appl. **19**, 122 (2013)

Tulasi Ram, S., Su, S.Y., Liu, C.H., Reinisch, B.W., McKinnell, L.A.: J. Geophys. Res. Space Phys. **114**, 1 (2009)

Vijayakumar, P.N., Pasricha, P.K.: Ann. Geophys. **15**, 345 (1997)

Wernik, A.W., Alfonsi, L., Materassi, M.: Acta Geophys. Pol. **52**, 238 (2004)

Wiens, R.H., Ledvina, B.M., Kintner, P.M., Afewerki, M., Mulugheta, Z.: Ann. Geophys. **24**, 1443 (2006)

Yeh, K.C., Soicher, H., Liu, C.H.: J. Geophys. Res. **84**, 6589 (1979)